Graphical abstract

Click here to access/download;Graphical abstract;Graphical Abstract 2(TIFF).tif

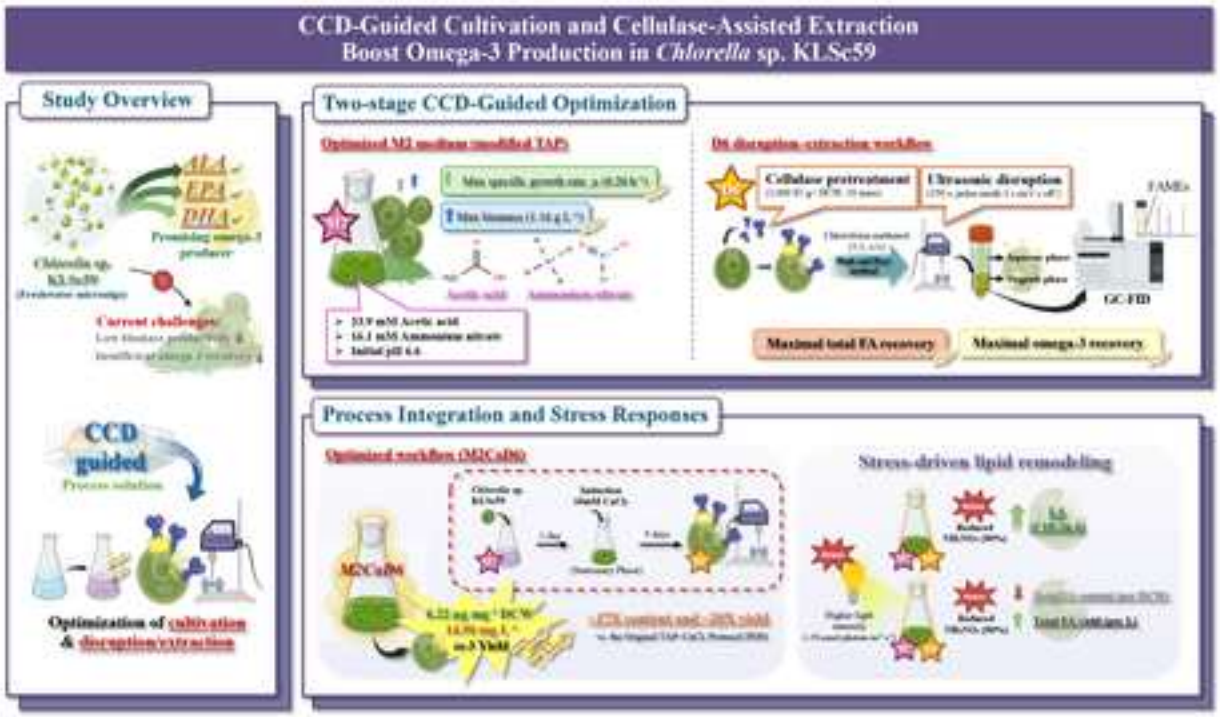

1. CCD optimized biomass production in *Chlorella* sp. KLSc59.
2. Cellulase-assisted sonication enhanced omega-3 extraction efficiency.
3. Integrated cultivation and extraction substantially increased omega-3 yield.
4. Nitrogen reduction and increased light altered fatty acid profiles.
5. The developed strategy provides a basis for scalable omega-3 bioprocesses.

Maximizing Omega-3 Production in *Chlorella* sp. KLSc59 through Central Composite Design-Driven Cultivation and Cellulase-Assisted Extraction

ABSTRACT

Chlorella sp. KLSc59 is a promising freshwater microalga for omega-3 oil production, but its application is limited by low biomass yield and inefficient lipid recovery. This study developed an integrated strategy to improve biomass production and omega-3 recovery. Carbon and nitrogen source screening in modified Tris-Acetate-Phosphate (TAP) medium identified acetic acid (CH_3COOH) and ammonium nitrate (NH_4NO_3) as the best-performing carbon and nitrogen sources. Central Composite Design (CCD) was then applied to optimize CH_3COOH and NH_4NO_3 concentrations and pH. The resulting M2 formulation (33.9 mM CH_3COOH, 16.1 mM NH_4NO_3, pH 6.6) gave the highest specific growth rate (0.20 h^{-1}) and biomass concentration (1.16 g L^{-1}) among the tested cultivation conditions. A second CCD was applied to optimize cell disruption by varying cellulase loading and sonication duration, identifying D6 (1,000 International Units (IU) g^{-1} DCW cellulase; 150 s sonication) as the best-performing extraction condition within the tested range for total and omega-3 fatty acid recovery. Among the tested comparative conditions, M2CaD6 yielded the highest omega-3 content and yield, increasing from 0.37 to 6.22 µg mg^{-1} DCW and from 0.74 to 14.90 mg L^{-1}, respectively, corresponding to 17- and 20-fold increases over the previous TAP-$CaCl_2$ cultivation and extraction method (PD0). Reducing NH_4NO_3 in M2 by half increased linoleic acid content, whereas higher light intensity (50 µmol m^{-2} s^{-1}) reduced cellular total fatty acid accumulation. Overall, coordinated optimization of cultivation, $CaCl_2$ induction, and enzymatic–mechanical disruption improved omega-3 production from *Chlorella* sp. KLSc59 and provides a basis for further process development.

Keywords: *Chlorella* sp. KLSc59; microalgae; omega-3 fatty acids; Central Composite Design; calcium induction; enzymatic cell disruption; lipid extraction

1. INTRODUCTION

Omega-3 polyunsaturated fatty acids (PUFAs), particularly eicosapentaenoic acid (EPA) and docosahexaenoic acid (DHA), have been extensively studied for cardiometabolic and anti-inflammatory benefits. Meta-analyses have shown that higher EPA and DHA consumption is associated with reduced triglyceride levels (Wang et al., 2023) and modest reductions in blood pressure (Miller et al., 2014), while systematic reviews indicate potential effects on inflammatory and oxidative-stress biomarkers (Natto et al., 2019; Innes and Calder, 2020). Increasing global demand for omega-3 oils has raised sustainability and safety concerns related to fish-derived sources, including overexploitation of marine fish stocks (FAO, 2024) and contamination risks in seafood and fish oils (Visciano, 2024). Microalgae constitute the primary producers of long-chain omega-3 PUFAs in aquatic food webs and therefore represent a sustainable alternative source for omega-3 oils in food, animal feed, and nutraceutical applications (Adarme-Vega et al., 2012; Hixson et al., 2015). Among them, *Chlorella* spp. are promising industrial candidates due to their rapid growth and adaptability to diverse cultivation modes (Moradi-Kheibari et al., 2022). Their lipid profiles are dominated by C16 and C18 fatty acids, including palmitic acid (C16:0) and α-linolenic acid (ALA; C18:3 n-3), which are relevant to nutritional and biofuel applications (Zibarev et al., 2024). *Chlorella* can be cultivated under photoautotrophic, mixotrophic, or heterotrophic conditions using organic carbon sources, enabling flexible process design and integration with low-cost or waste-derived substrates (Manhaeghe et al., 2020; Perez-Garcia, 2011a; Perez-Garcia, 2011b). However, long-chain omega-3 polyunsaturated fatty acids, particularly EPA and DHA, are typically associated with specific, predominantly marine microalgae, indicating that omega-3 production in *Chlorella* may require careful strain selection and targeted process optimization (Adarme-Vega et al., 2012). Consequently, maximizing omega-3 oil yields from *Chlorella*-based bioprocesses necessitates coordinated optimization of upstream biomass production and downstream cell disruption and lipid extraction strategies (Oh et al., 2022; Geada et al., 2023).

Carbon and nitrogen availability strongly influence microalgal growth, biomass composition, productivity, and overall process economics (Nayak et al., 2019; Maltsev et al., 2023). During nutrient-replete growth, nitrogen supports protein synthesis, pigment accumulation, and rapid cell division (Maltsev et al., 2023), whereas nitrogen limitation suppresses protein and pigment biosynthesis and redirects cellular carbon toward neutral lipid storage, primarily as triacylglycerols (TAGs), with species- and stress-dependent changes in fatty acid composition (Mujtaba et al., 2012; Wang et al., 2019b; Liu et al., 2016). Strategies such as two-stage nitrogen step-down cultivation, optimization of nitrogen source and concentration, and manipulation of salinity and light intensity have been employed to enhance lipid accumulation (Mujtaba et al., 2012; Nayak et al., 2019; Shi et al., 2020). However, stress-induced lipid accumulation is often accompanied by reduced biomass productivity, limiting gains in total lipid and omega-3 PUFA yields (Wang et al., 2019b; Liu et al., 2016; Adams et al., 2013). Consequently, developing scalable cultivation strategies that balance high biomass production with targeted omega-3 enrichment remains a key challenge (Adams et al., 2013; Liu et al., 2016; Shi et al., 2020). The use of readily assimilable organic carbon sources such as acetate and glycerol enables mixotrophic or heterotrophic cultivation, which can enhance *Chlorella* biomass and lipid accumulation compared with photoautotrophic growth (Liang et al., 2009; Xie et al., 2020; Chen and Walker, 2011). In parallel, nitrogen sources, including ammonium, nitrate, and urea, influence growth performance, pigment content, and lipid accumulation and composition in green microalgae (González-Garcinuño et al., 2014; Ziganshina et al., 2022). While several studies have combined

carbon-nitrogen strategies to enhance lipid productivity, strain-specific optimization for omega-3 production remains limited, and systematic investigations into carbon-nitrogen combinations targeting omega-3 profiles are lacking.

Beyond cultivation, downstream processing presents a major bottleneck for omega-3 recovery from *Chlorella*, as its robust and chemically resistant cell wall restricts lipid accessibility (Oh et al., 2022; Weber, 2022). The cell walls of green coccoid microalgae contain polysaccharides, complex carbohydrates, and glycoproteins, and, in some taxa, highly resistant aliphatic biopolymers such as algaenan (Chen et al., 2018; Zych, 2022). Inadequate cell disruption can significantly reduce lipid extraction efficiency (Chen et al., 2018; Oh et al., 2022). Mechanical, chemical, and biological pretreatments, including bead milling, high-pressure homogenization, sonication, alkaline or acid treatments, and enzymatic hydrolysis, vary in energy demand, scalability, and impact on product quality (Günerken et al., 2015; Oh et al., 2022). Enzyme-assisted pretreatment using cellulases has been shown to enhance lipid extraction by partially hydrolyzing carbohydrate-rich wall components in *Chlorella* and other green algae (Zuorro et al., 2019; Liang et al., 2012), while combined strategies integrating enzymatic hydrolysis with moderate mechanical disruption can further improve extraction efficiency while reducing energy input (Alavijeh et al., 2020; Rahman et al., 2022; Liu et al., 2022b). Because ultrasonic treatment may generate heat and reactive species that compromise oxidation-sensitive PUFAs, enzymatic pretreatment coupled with milder sonication is often preferred (Liu et al., 2022b; Gerde et al., 2012). The effectiveness of such approaches depends on strain-specific cell wall properties and cultivation conditions, and optimal parameters for omega-3 extraction from *Chlorella* remain poorly defined (Zuorro et al., 2019; Rahman et al., 2022; Liu et al., 2022b). CCD-based response surface methodology (RSM) offers a powerful tool to optimize both upstream cultivation and downstream extraction while minimizing experimental burden and revealing key variable interactions. Previous studies have shown that CCD is effective for optimizing microalgal cultivation variables and medium composition, resulting in improved biomass production and target metabolite accumulation under mixotrophic conditions (Do et al., 2022; Rincon et al., 2024). Specifically, CCD has been used to optimize nutrient and cultivation parameters for enhanced biomass and lutein production in *Chlorella sorokiniana* (Do et al., 2022) and to identify medium compositions that support high biomass and lipid-related performance in *Chlorella vulgaris* (Rincon et al., 2024). In downstream processing, CCD has also been applied to optimize ultrasonic pretreatment and extraction parameters, leading to substantially improved lipid recovery (Ellison et al., 2019; Hadrich et al., 2018). However, integrated CCD-based optimization specifically targeting omega-3-rich oil production remains limited.

Previous studies demonstrated that *Chlorella* sp. KLSc59 produces ALA and detectable levels of EPA and DHA under TAP cultivation, with omega-3 yields enhanced by calcium chloride ($CaCl_2$) supplementation (Preechaphonkul et al., 2024; Shim et al., 2020). Building on this foundation, this study aimed to develop an integrated CCD-guided cultivation and cellulase-assisted extraction strategy to enhance omega-3 oil yield from *Chlorella* sp. KLSc59, by optimizing carbon and nitrogen sources, refining disruption conditions, and evaluating combined cultivation and lipid extraction approaches relative to previously reported protocols (Preechaphonkul et al., 2024).

2. MATERIAL AND METHODS

2.1 Algal Strain and Cultivation Conditions

The green microalga *Chlorella* sp. KLSc59 was isolated and taxonomically characterized as previously described by Sirawattanamongkol et al. (2020). Stock cultures were maintained in TAP medium and periodically subcultured to ensure sustained exponential growth. Cultivation experiments were conducted in 100-mL Erlenmeyer flasks containing 50 mL of medium, incubated at 30°C under continuous white light with orbital shaking at 130 rpm. All media were sterilized by autoclaving at 121°C for 15 minutes prior to use. For carbon- and nitrogen-source screening experiments (Section 2.3), cultures were inoculated to an initial optical density at 750 nm (OD_{750}) of 0.05 to facilitate comparative evaluation of growth under different nutrient conditions. For biomass optimization using CCD (Section 2.4) and all subsequent lipid extraction experiments (Sections 2.5-2.6), cultures were inoculated at an initial OD_{750} of 0.10 to ensure consistency across experiments and to obtain sufficient biomass for further analysis.

Carbon- and nitrogen-source screening and CCD-based biomass optimization experiments were performed under continuous white light at approximately 50 µmol photons m^{-2} s^{-1}, whereas the subsequent comparative cultivation and extraction-related experiments were conducted under approximately 5 µmol photons m^{-2} s^{-1} to maintain consistency with the cultivation framework adopted from the previous KLSc59 study. Screening and biomass-stage CCD experiments were used to select cultivation inputs for biomass optimization, while the subsequent comparative experiments were conducted under the low-light framework adopted from the previous KLSc59 study to evaluate integrated production strategies.

2.2 Culture Media and Reagents

TAP medium was prepared according to standard TAP formulation described by Andersen (2005), Gorman and Levine (1965), Harris (1989), and Sueoka (1960). Carbon-free TAP (TAP-C) and nitrogen-free TAP (TAP-N) were prepared to assess the influence of specific nutrients on biomass production. TAP-C was formulated by omitting acetic acid from the standard TAP recipe, whereas TAP-N was prepared by replacing ammonium chloride with sodium chloride and ammonium molybdate with sodium molybdate at equivalent molar concentrations in order to maintain ionic strength while eliminating combined nitrogen sources.

For carbon-source screening, TAP-C was supplemented with individual carbon sources at concentrations ranging from 10 to 40 mM, including acetic acid, glycerol, ethanol, sodium carbonate, acetone, *n*-propanol, and propionic acid. Volatile carbon sources, including ethanol, acetone, and *n*-propanol, were sterilized by filtration through 0.22-µm PTFE membrane filters and aseptically added to autoclaved TAP-C medium. Nitrogen-source screening was performed by supplementing TAP-N with ammonium chloride, ammonium nitrate, ammonium sulphate, potassium nitrate, sodium nitrate, sodium nitrite, thiourea, or urea at concentrations ranging from 10 to 40 mM. Standard TAP medium, TAP-C, and TAP-N were used as controls.

For calcium induction experiments, analytical-grade $CaCl_2$ was prepared as a sterile stock solution and added to cultures at a final concentration of 10 mM. Commercial cellulase (CTi and Science Co., Ltd., CAS 9012-54-8) was utilized for enzymatic cell disruption. Methanol, chloroform, and hexane (HPLC grade) were used for lipid extraction.

2.3 Comparison of Carbon and Nitrogen Sources

Cultures were inoculated to an initial OD_{750} of 0.05 and incubated for 7 days under the cultivation conditions described in section 2.1. Cell growth was monitored daily by measuring OD_{750}. Specific growth rates (µ, h^{-1}) were calculated during the exponential phase using the equation $\mu = (\ln X_2 - \ln X_1)/(t_2 - t_1)$, where X_1 and X_2 represent the optical densities at times t_1

and t_2, respectively (Sekine et al., 2020). Carbon and nitrogen sources that produced the highest specific growth rates and consistent growth profiles were selected for subsequent CCD-based optimization.

2.4 Optimization of Biomass Production Using CCD

Based on the screening results, acetic acid and ammonium nitrate were selected as the carbon and nitrogen sources, respectively, for biomass production. A three-factor CCD was employed to optimize biomass production in modified TAP medium by evaluating the effects of acetic acid concentration (A), ammonium nitrate concentration (B), and initial pH (C), with an axial distance of 1.6817. The CCD data for biomass production were fitted to the second-order polynomial regression model described in Section 2.9. The coded and actual levels of each variable and the experimental design matrix were specified for the biomass-stage CCD. The biomass-stage CCD comprised 15 design points, including one center-point condition (M15). All CCD conditions, including the center point, were evaluated in biological triplicate. Initial pH values were adjusted using 1 M HCl or NaOH solutions prior to autoclaving. Standard TAP medium was used as a reference control.

For each CCD condition, cultures were inoculated to an initial OD_{750} of 0.10 and incubated for 7 days. Optical density was measured daily to generate growth curves. Specific growth rate and doubling time (Td) were calculated from the exponential growth phase described in section 2.3. Dry cell weight (DCW, g L^{-1}) was determined by harvesting culture on day 7 via centrifugation (4,500 rpm, 5 min), rinsed pellets with distilled water, and dried at 60°C until a constant weight was achieved. Total chlorophyll content was quantified spectrophotometrically from 90% (v/v) methanol extracts using the equations described by Ritchie (2008). CCD data were utilized to generate response surface plots illustrating the effects of acetic acid concentration, ammonium nitrate concentration, and pH on specific growth rate. For CCD-based statistical modelling of the biomass-stage experiments, specific growth rate was used as the primary modeled response. Dry cell weight and total chlorophyll content were evaluated as supporting biomass-related outcomes for interpretation of the selected cultivation condition.

2.5 Cultivation Conditions for Omega-3 Enhancement and Comparative Production

Multiple cultivation and extraction strategies were established to compare omega-3 production under different upstream and downstream conditions, including the previously reported TAP-based protocol (Preechaphonkul et al., 2024), the optimized cultivation medium developed in this study, and the optimized cell disruption and lipid extraction method identified in this work. In the previous condition (P), cells were cultured in TAP medium supplemented with 10 mM $CaCl_2$ throughout the culture period. Biomass from this condition was extracted using either the original extraction method (PD0) or the optimized cell disruption and lipid extraction method developed in this study (PD6).

Additional cultivation strategies integrating TAP or M2 medium, $CaCl_2$ induction, and the optimized D6 extraction were performed. TAPD6 consisted of cells cultivated in TAP medium without Ca^{2+} supplementation and extracted using D6. For TAPCaD6, cells were cultivated in TAP medium until day 1 (early stationary phase), followed by supplementation with 10 mM $CaCl_2$ and an additional 5 days of cultivation prior to extraction using D6. M2CaD6 consisted of cells cultivated in the optimized M2 medium (CCD condition M2: 33.9 mM acetic acid, 16.1 mM ammonium nitrate, initial pH 6.6) until day 1 (early stationary phase), followed by $CaCl_2$ induction (10 mM) and an additional 5 days of cultivation before extraction using D6.

To evaluate the effects of nitrogen limitation and increased light intensity, two stress conditions were developed. In M2CaND6, the ammonium nitrate concentration in M2 medium was reduced by 50% (from 16.1 to 8.05 mM), while $CaCl_2$ induction and cultivation duration remained unchanged. In M2CaNLD6, the same nitrogen-reduced medium was used with $CaCl_2$ induction, and light intensity was 50 µmol photons m^{-2} s^{-1}. Biomass from all conditions was harvested on the final cultivation day and subjected to D6 extraction. Total fatty acid content, fatty acid composition, omega-3 yield, total lipid weight, and cellular morphology were subsequently analyzed. These comparative conditions were selected to evaluate representative cultivation-extraction workflows relative to the previous KLSc59 protocol and to the process modifications developed in the present study.

2.6 Optimization of Cell Disruption and Lipid Extraction Using CCD

A two-factor CCD was applied to optimize cell disruption and lipid extraction by evaluating the effects of cellulase loading (A) and sonication time (B), with an axial distance of 1.414. The CCD data for extraction optimization were fitted to the second-order polynomial regression model described in Section 2.9, and model performance and adequacy were evaluated in the subsequent statistical analysis. The coded and actual levels of these variables and the experimental matrix were specified for the extraction-stage CCD. The extraction-stage CCD comprised 9 design points, including one center-point condition (D9). All CCD conditions, including the center point, were evaluated in biological triplicate. Cells cultivated in the optimized M2 medium were harvested by centrifugation (4,500 rpm, 5 min), washed with distilled water, and resuspended in 10 mM acetate buffer (pH 5.0). Aliquots corresponding to 100 mg DCW were transferred to reaction tubes and supplemented with cellulase according to the CCD design. Enzymatic hydrolysis was carried out at 50°C for 10 min to partially degrade carbohydrate-rich cell wall components, based on manufacturer recommendations and preliminary optimization.

Lipid extraction was performed using a modified Bligh and Dyer method (Bligh and Dyer, 1959). Chloroform:methanol (1:1, v/v) was added at four times the suspension volume, and the samples were vortex-mixed prior to sonication. Sonication was conducted according to the CCD design (0–300 s, pulse mode 1 s on/1 s off) using a probe sonicator (VCX 500, 500 W, 20 kHz; Sonics & Materials, Inc., Newtown, CT, USA). Following centrifugation (4,500 rpm for 5 min, 25°C), the lower chloroform phase was carefully collected and evaporated under a gentle nitrogen stream to obtain crude lipid extracts. Extracted lipids were weighed and used for FAME preparation and GC-FID analysis.

2.7 Preparation of FAME and GC-FID Analysis

Dried lipid extracts were reconstituted in 1 mL of hexane and vortexed for 1 min. Transesterification was initiated by adding 200 µL of 25% (w/v) sodium methoxide in methanol, followed by incubation at 50°C for 5 min. After cooling to room temperature, samples were centrifuged at 6,500 rpm for 5 min, and the clear upper phase containing FAMEs was collected for further analysis.

Fatty acid analysis was performed using a gas chromatograph equipped with a flame ionization detector (Nexis GC-2030, Shimadzu Corporation, Japan). FAMEs were separated on a DB-23 capillary column (30 m x 0.25 mm i.d., 0.25 µm film thickness; Agilent, USA). The oven temperature was initially maintained at 50°C for 0.5 minutes, increased to 150°C at 25°C min^{-1}, raised to 174°C at 2.3°C min^{-1}, and finally increased to 220°C at 2.0°C min^{-1}, where it was held for 3 min. Injector and detector temperatures were set according to the manufacturer's

recommendation. Helium was used as the carrier gas, while nitrogen served as the makeup gas. Individual fatty acids were identified by comparing their retention times with those of the Supelco 37 Component FAME Mix. Relative fatty acid composition was determined by peak area normalization and expressed as the percentage of total detected fatty acids. Total fatty acid content (μg mg^{-1} DCW) and yield (mg L^{-1}) were calculated from the sum of all quantified FAMEs detected in each sample and normalized to dry cell weight and culture volume, respectively. Fatty acids were categorized as saturated (SAT: C14:0, C16:0, C17:0, C18:0), monounsaturated (MUFA: C16:1, C17:1, C18:1), linoleic acid (LA, C18:2 n-6), and omega-3 fatty acids (C18:3 n-3, C20:5 n-3, C22:6 n-3). SAT, MUFA, LA, and omega-3 fatty acids were reported separately for compositional analysis.

2.8 Microscopic and Cellular Analysis

Microscopic observations were conducted on samples collected on the final day of cultivation for each experimental condition. Aliquots of culture were loaded onto a hemacytometer and examined using a bright-field microscope equipped with a digital camera. High magnification images were captured to evaluate cell morphology and aggregation behavior.

For quantitative cell size analysis, at least 30 individual cells per condition were randomly selected from micrographs, and cell diameters were measured using the calibrated hemacytometer scale. Mean cell diameter and standard deviation were calculated to compare cell-size distributions across cultivation conditions.

2.9 Statistical Analysis

All experiments were performed in triplicate, and data were presented as mean ± standard deviation. Statistical significance among treatments was assessed using one-way analysis of variance (ANOVA) at a 95% confidence level. When significant differences were detected ($p < 0.05$), Tukey's honestly significant difference (HSD) post hoc test was applied.

For CCD-based optimization, the experimental data were fitted to a second-order polynomial regression model using the following equation:

$$Y = \beta_0 + \sum_{i=1}^{k} \beta_i x_i + \sum_{i=1}^{k} \beta_{ii} x_i^2 + \sum_{i<j} \beta_{ij} x_i x_j \quad (1)$$

where Y is the predicted response, β_0 is the intercept, β_i represents the linear coefficients, β_{ii} represents the quadratic coefficients, β_{ij} represents the interaction coefficients, and x_i and x_j are the independent variables.

For the biomass-stage CCD, specific growth rate was used as the modeled response, whereas total fatty acid content was used as the modeled response for the extraction-stage CCD. Model adequacy was evaluated using ANOVA, including overall model significance and lack-of-fit testing. The coefficient of determination (R^2), adjusted R^2, root mean square error (RMSE), and coefficient of variation (CV%) were used to assess model performance. Residual plots, histogram, and Q-Q plot were additionally examined to assess residual behavior. CCD model fitting and lack-of-fit analyses were performed in JMP software (version 19.1.1), while residual diagnostics were additionally examined using JASP software (version 0.95.1). Full ANOVA tables, model coefficients, model adequacy statistics, and residual diagnostics were compiled for both CCD models.

3. RESULTS AND DISCUSSION

3.1 Effect of carbon and nitrogen sources on biomass production

Carbon and nitrogen availability strongly influence microalgal growth and metabolism, particularly under mixotrophic conditions (Cecchin et al., 2018). In standard TAP medium, acetic acid (17 mM) serves as a primary organic carbon source, whereas carbon-free TAP (TAP-C) was used as a negative control. Screening of multiple carbon sources (10-40 mM) revealed that acetic acid supported markedly superior growth compared with carbonate, alcohols, ketones, and glycerol (Fig. 1A-C). Cultures supplied with acetic acid rapidly entered stationary phase within 24 h and exhibited the highest specific growth rates (μ = 0.09-0.12 h^{-1}), whereas other carbon sources (ethanol, propanol, acetone, glycerol) supported only limited growth (μ = 0.02-0.06 h^{-1}), comparable to TAP-C (Fig. 1A-B). By day 7, acetate-grown cultures were visibly denser and darker green (Fig. 1C), consistent with higher biomass accumulation.

The superior performance of acetic acid is attributed to its role as a readily assimilable C_2 substrate that is rapidly converted to acetyl-CoA and funneled into central carbon metabolism, specifically the TCA cycle and glyoxylate pathway, thus providing energy and biosynthetic precursors essential for biomass formation (Cai et al., 2022; Cecchin et al., 2018). In *Chlorella*, acetate utilization is intimately related to glyoxylate cycle stimulation; particularly, isocitrate lyase (ICL), a key enzyme in this cycle, is upregulated in acetate-adapted cells (John and Syrett, 1967). This induction indicates that when acetate is the predominant carbon source, *Chlorella* effectively diverts carbon flux at the isocitrate branch point from the complete TCA cycle to the glyoxylate pathway. ICL converts isocitrate to succinate and glyoxylate, bypassing the CO_2-releasing decarboxylation steps of the TCA cycle. This preserves carbon skeletons for biosynthesis and biomass accumulation. The higher ICL level in acetate-adapted cells implies that the glyoxylate cycle is a crucial metabolic mechanism for effective growth on a C_2 substrate like acetate (John and Syrett, 1967). Carbonate, on the other hand, is an inorganic carbon source that promotes development mostly by photosynthetic inorganic carbon assimilation (Calvin cycle), rather than directly providing reduced carbon (Shelp and Canvin, 1980). Under limited light/CO_2 fixation, it is expected to perform similarly or slightly better than the organic carbon-free control. In contrast, the investigated C_2/C_3 alcohols and ketone (ethanol, propanol, and acetone) require additional oxidation processes and exhibit solvent toxicity before being incorporated into central metabolism, resulting in lower growth performance compared to acetate (Catalanotti et al., 2013; Miazek et al., 2017). Finally, while glycerol can facilitate mixotrophic growth in certain *Chlorella* strains, its absorption and catabolic efficiency are dependent on species/strain variations and may be influenced by concentration and transport limitations, potentially explaining the restricted growth observed in comparison to acetate (Liang et al., 2009; Heredia-Arroyo et al., 2011; Perez-Garcia et al., 2011a).

Nitrogen-sources screening showed that potassium nitrate, urea, sodium nitrate, ammonium sulphate, ammonium chloride, and ammonium nitrate supported comparable growth across all tested concentrations, yielding similar specific growth rates (μ = 0.12-0.13 h^{-1}) and dark green culture by day 7 (Fig. 2A-C). In contrast, nitrogen-free TAP (TAP-N) resulted in significantly reduced growth (μ = 0.07 h^{-1}) (Fig. 2B). This comparable performance reflects the metabolic versatility of *Chlorella* in nitrogen assimilation; NH_4^+ is directly assimilated, whereas NO_3^- utilization requires inducible nitrate reductase and is tightly regulated by ammonium availability. Notably, *Chlorella* grown on ammonium nitrate preferentially assimilates NH_4^+, with nitrate assimilation resuming following ammonium depletion (Morris and Syrett, 1963; Syrett and Morris, 1963). Urea also supported growth, consistent with early biochemical studies

demonstrating urea assimilation by *Chlorella* cells. (Hattori, 1957). In contrast, thiourea and sodium nitrite resulted in markedly reduced growth compared with the aforementioned nitrogen sources and even lower growth than TAP-N (Fig. 2A), with μ values ranging from 0.03 to 0.05 h^{-1} (Fig. 2B). The pale and comparatively clear cultures observed on day 7 cultures further confirmed growth inhibition (Fig. 2C). In *Chlorella fusca*, thiourea uptake occurs via proton co-transport, potentially imposing energetic and proton-balance constraints that limit efficient nitrogen assimilation (Rees and Syrett, 1984). In *Chlorella vulgaris*, nitrite addition has been reported to suppress growth even when total nitrogen levels are maintained, indicating nitrite-induced stress (Pozzobon et al., 2021).

Although multiple nitrogen sources supported comparable growth, ammonium nitrate was chosen for subsequent cultivation. Ammonium nitrate supplies two nitrogen atoms at different redox states (NH_4^+ and NO_3^-), enabling rapid ammonium assimilation followed by nitrate utilization once ammonium becomes limiting (Syrett and Morris, 1963). Importantly, mixed NH_4^+/NO_3^- assimilation can mitigate pH fluctuations associated with nitrogen uptake, as the opposing proton fluxes partially counterbalance one another, thereby stabilizing culture pH at high growth rates (Scherholz and Curtis, 2013). Accordingly, acetic acid and ammonium nitrate were selected to formulate a modified TAP medium for subsequent experiments.

3.2 Biomass-Stage Optimization for Biomass Production

Following preliminary screening, acetic acid and ammonium nitrate were identified as suitable carbon and nitrogen sources, respectively, for *Chlorella* sp. KLSc59. A three-factor CCD was used to optimize biomass production by varying acetic acid (10-40 mM), ammonium nitrate (10-40 mM), and initial pH (6.0-9.0) in modified TAP medium, with standard TAP serving as the reference control. The CCD comprised 15 experimental conditions (M1-M15), informed by preliminary data and literature. Growth profiles revealed that several conditions, particularly M2, M4, M6, M10, and M11, promoted rapid biomass accumulation within the first 24 h relative to TAP (Fig. 3A). These conditions exhibited significantly improved kinetic parameters compared with the TAP control ($\mu = 0.15 \pm 0.01$ h^{-1}; $Td = 4.57 \pm 0.19$ h), with M2, M4 and M10 showing the highest growth rates ($\mu = 0.18$-0.20 h^{-1}; $Td = 3.51$-3.77 h) (Fig. 3C-D). Distinct color variations among day-7 cultures (Fig. 3B) suggest differential physiological responses, including changes in pigment composition and intracellular organization, consistent with the metabolic adaptability of *Chlorella* during mixotrophic and nitrogen-responsive conditions (Cecchin et al., 2018; Markou et al., 2017; Liu et al., 2022a).

Despite rapid early growth, certain conditions (notably M4, M6, and M10) exhibited late-stage declines in optical density and total chlorophyll content by day 7, relative to TAP. This pattern suggests a transition from early proliferation to stress-limited growth, likely driven by condition-specific constraints related to pH, carbon availability, and nitrogen assimilation (Qiu et al., 2017; Markou et al., 2017; Liu et al., 2022a). Integrated evaluation of μ, Td, DCW, and total chlorophyll content identified M2 as the best-performing condition under the tested conditions. M2 (33.9 mM acetic acid, 16.1 mM ammonium nitrate, initial pH 6.6) achieved the highest specific growth rate ($\mu = 0.20 \pm 0.01$ h^{-1}), shortest doubling time ($Td = 3.51 \pm 0.10$ h), highest DCW (1.16 g L^{-1}), and highest total chlorophyll content (16.09 mg L^{-1}), all significantly exceeding the other CCD conditions and the TAP control (Fig. 3C-F).

To further evaluate the combined effects of acetic acid concentration (A), ammonium nitrate concentration (B), and initial pH (C) on specific growth rate, the CCD data were analyzed using a second-order polynomial regression model. The overall model was significant ($F = 36.81$,

$p < 0.0001$), with an R^2 of 0.9045 and an adjusted R^2 of 0.8799, indicating that the model explained a large proportion of the variation in the response. The RMSE was 0.0092, corresponding to a CV of approximately 5.95%. Among the fitted terms, A, C, AB, AC, BC and C^2 were significant. However, the lack-of-fit test was also significant ($p < 0.0001$), indicating that although the quadratic model captured most of the variation in specific growth rate, it did not fully describe the response surface across the investigated design space. This limitation should be considered when interpreting the biomass-stage CCD model. The fitted regression equation for specific growth rate was:

$$\mu\ (h^{-1}) = 0.1630 + 0.0189(A) - 0.0026(B) - 0.0130(C) - 0.0039(AB) - 0.0103(AC) - 0.0038(BC) - 0.0034(A^2) + 0.0023(B^2) - 0.0082(C^2) \quad (2)$$

The positive coefficient of A suggested that increasing acetic acid concentration promoted growth within the tested range, whereas the negative coefficients of C, AC, and C^2 indicated that pH and its interaction structure contributed negatively to specific growth rate within the investigated region. The superior performance of M2 likely reflects a favorable balance among carbon supply, nitrogen availability, and pH. Acetate provides a reduced carbon source readily assimilated as acetyl-CoA, supporting biomass formation under mixotrophic conditions. In *Chlorella*, acetate metabolism involves glyoxylate-cycle activity, particularly ICL, facilitating incorporation of acetate-derived carbon into biomass precursors (John and Syrett, 1967; Cecchin et al., 2018). Moreover, the supplemented acetic acid and ammonium nitrate in M2 corresponded to an estimated molar C:N ratio of approximately 2.1:1, supplying sufficient carbon skeletons and nitrogen for sustained protein and chlorophyll synthesis without inducing late-stage imbalance (Cecchin et al., 2018; Markou et al., 2017). The initial pH of 6.6 in M2 likely provided a favorable balance between inorganic carbon availability and acetate tolerance. Relative to more alkaline conditions, pH 6.6 would increase dissolved CO_2 availability and support RuBisCO carboxylation. However, because lower pH increases the fraction of undissociated acetic acid, this benefit is interpreted as a compromise between CO_2 supply and acid-associated stress rather than a simple minimization of both constraints (Dickson et al., 2007; Zeebe and Wolf-Gladrow, 2001; Giordano et al., 2005; Lacroux et al., 2021). Additionally, mixed NH_4^+/NO_3^- assimilation can stabilize culture pH through counterbalancing proton fluxes, an advantage emphasized for high-density algal cultivation (Scherholz and Curtis, 2013). M2 was selected from the biomass-stage CCD conducted at 50 µmol photons m^{-2} s^{-1} and was subsequently carried forward to the comparative production experiments performed under the low-light framework adopted from the previous KLSc59 study. The present results therefore support M2 as the best-performing cultivation condition within the biomass-stage optimization context, while its performance across different light regimes remains to be verified.

In contrast, late-stage decline in certain CCD conditions reflected specific factor-dependent response patterns, particularly M4 (33.9 mM acetic acid, 33.9 mM ammonium nitrate, pH 6.6), M6 (33.9 mM acetic acid, 16.1 mM ammonium nitrate, pH 8.4), and M10 (40.0 mM acetic acid, 25.0 mM ammonium nitrate, pH 7.5). Elevated initial pH (M6) likely reduced CO_2 availability and increased energetic costs for pH homeostasis, limiting growth and pigment maintenance at later phases, consistent with reported alkaline stress responses in *Chlorella* (Qiu et al., 2017; Guckert and Cooksey, 1990). High acetic acid levels in M10 may accelerate early mixotrophic growth (Lacroux et al., 2021) but subsequently induce organic-acid stress, influenced by the undissociated acid fraction and dependent on both acetic acid concentration and pH (Lacroux et al., 2020;

Lacroux et al., 2021). Similarly, late-stage inhibition under the high ammonium nitrate condition (M4) may reflect nitrogen-associated pH imbalance in mixotrophic *Chlorella*, as ammonium-dominated assimilation can contribute to culture pH shifts, whereas balanced NH_4^+/NO_3^- utilization has been proposed to minimize pH fluctuations in high-density algal cultivation (Scherholz and Curtis, 2013), consistent with reports of ammonium-associated inhibition of photosynthesis in *Chlorella* (Wang et al., 2019a).

The second-order polynomial regression model and response surface analysis generally supported these observations (Fig. 3G), indicating acetic acid concentration as the dominant positive factor influencing growth, with favorable performance observed within the tested conditions, particularly at pH 6.0-7.0 and acetic acid concentrations above 30 mM. Nitrogen effects were comparatively moderate, consistent with partial buffering by mixed NH_4^+/NO_3^- assimilation (Lacroux et al., 2020; Scherholz and Curtis, 2013).

3.3 Extraction-Stage Optimization for Fatty Acid Extraction and Omega-3 Recovery

Following biomass optimization under M2 growth conditions, cell disruption and lipid extraction were optimized using a two-factor CCD by varying cellulase activity (500-1,000 IU g^{-1} DCW) and probe-sonication duration (50-300 s). These variables were selected because lipid recovery from *Chlorella* is often limited by its robust, polysaccharide-rich cell wall, and enzymatic pretreatment can reduce mechanical energy requirements while enhancing solvent access to intracellular lipids (Günerken et al., 2015; Oh et al., 2022). Cellulase partially hydrolyzes cell-wall polysaccharides, increasing permeability and facilitating lipid release (Cho et al., 2013), whereas sonication provides cavitation-driven shear forces that rupture weakened cell envelopes. However, excessive sonication may generate localized heating and free radicals, accelerating PUFA oxidation and degradation (Gerde et al., 2012; Günerken et al., 2015).

Across the nine disruption conditions (D1-D9), the relative fatty acid class distribution remained largely conserved (Fig. 4A), with LA (~34%) predominating, followed by SAT (~31%), total omega-3 (~18%), and MUFA (~17%), while the omega-3 fraction was dominated by ALA, with EPA and DHA detected at lower levels. In contrast, biomass-normalized fatty acid contents varied substantially: total fatty acid contents ranged from 17.34 to 39.16 μg mg^{-1} DCW, whereas total omega-3 contents ranged from 2.09 to 4.23 μg mg^{-1} DCW (Fig. 4B). Analysis of the individual omega-3 components revealed that ALA predominated, whereas EPA and DHA were present only at lower levels (Fig. 4C). Although D2 and D6 produced comparable total fatty acid recoveries, D6 achieved the highest omega-3 content (4.23 ± 0.64 μg mg^{-1} DCW) and was therefore selected as the best-performing condition within the tested range.

To further evaluate the combined effects of cellulase loading (A) and sonication duration (B) on total fatty acid content, the CCD data were analyzed using a second-order polynomial regression model. The overall model was significant ($F = 21.47$, $p < 0.0001$), with an R^2 of 0.8364 and an adjusted R^2 of 0.7975, indicating that the model explained a substantial proportion of the variation in the response. The RMSE was 3.2126, corresponding to a CV of approximately 12.53%. Among the fitted terms, A, AB, and A^2 were significant, whereas B and B^2 were not significant. In addition, the lack-of-fit test was not significant ($p = 0.0848$), supporting the adequacy of the fitted quadratic model within the investigated design space. The fitted regression equation for total fatty acid content was:

$$\text{Total fatty acid content } (\mu g\ mg^{-1}\ DCW) = 22.3414 + 5.7506A - 0.0553B - 4.6340AB + 2.5013A^2 + 1.2112B^2 \quad (3)$$

The positive coefficient of A indicated that cellulase loading positively influenced total fatty acid extraction efficiency within the tested range, while the significant interaction term (AB) suggested that the effect of cellulase depended on the applied sonication time.

Response-surface modeling placed D2 and D6 in the high-recovery region observed within the investigated design space (Fig. 4D), indicating a strong positive effect of cellulase loading. Although the fitted surface suggested favorable performance at high cellulase loading and relatively short sonication, this region was interpreted cautiously, as optimization prioritized omega-3 yield and reproducibility rather than total fatty acids alone. Enzymatic wall weakening followed by moderate sonication may improve disruption efficiency and solvent penetration, while more severe sonication conditions have been associated with localized heating and oxidative degradation of PUFAs (Gerde et al., 2012; Günerken et al., 2015). D6 appears to represent a practical balance in which elevated cellulase improves cell-wall permeability and lipid accessibility (Cho et al., 2013; Zuorro et al., 2019), while moderate sonication likely facilitated lipid release under the tested conditions. This interpretation is consistent with previous reports that enzyme-assisted pretreatment can enhance lipid extraction in *Chlorella*, whereas excessive sonication may compromise PUFA integrity (Cho et al., 2013; Gerde et al., 2012). However, no direct oxidation measurements were performed in the present study. Therefore, the current results do not provide direct evidence that D6 preserved PUFA integrity relative to more severe sonication conditions. Accordingly, D6 (1,000 IU g^{-1} DCW cellulase; 150 s sonication) was selected as the best-performing condition within the tested range, providing high total fatty acid recovery, the highest omega-3 content, and low variability.

3.4 Effects of cultivation and disruption strategies on fatty acid and omega-3 production

To benchmark the optimized workflow against the previous protocol and evaluate stress-driven responses, fatty acid and omega-3 production was compared across cultivation and cell disruption strategies in *Chlorella* sp. KLSc59. This design aimed to isolate the effects of (i) cultivation optimization, (ii) cell disruption and lipid extraction efficiency, and (iii) physiological responses to nitrogen limitation and elevated light intensity. Stress testing was motivated by evidence that *Chlorella* remodels lipid metabolism under nitrogen depletion and/or high light, promoting TAG accumulation, altering desaturation profiles, and inducing thylakoid and redox-associated responses (Goncalves et al., 2013; Guo et al., 2015; Vijayan et al., 2024; Wang and Miao, 2022).

To assess disruption efficiency, PD0 and PD6 were compared under identical baseline cultivation (P). With equal biomass input, D6 recovered ~2.3-fold higher total fatty acid content than D0 (Fig. 5A) and showed a 1.8-fold increase in average omega-3 recovery, although the latter was not statistically significant. This improvement reflects enhanced cell-wall weakening and lipid accessibility in D6, consistent with reports linking improved disruption to increased lipid extractability in *Chlorella* (Günerken et al., 2015; Oh et al., 2022). Unlike the reference D0 protocol relying solely on prolonged ultrasonication, followed by chloroform-methanol extraction using a separatory funnel and subsequent base-catalyzed transesterification (Preechaphonkul et al., 2024), D6 employs enzyme-assisted pretreatment followed by controlled probe sonication, providing a mechanistic basis for its superior fatty acid recovery.

To assess Ca^{2+} adaptation, TAPD6 and TAPCaD6 were compared. $CaCl_2$ supplementation significantly increased total fatty acid accumulation while leaving omega-3 content unchanged, but it altered fatty acid composition, notably increasing linoleic acid (Fig. 5A). Ca^{2+}-supplemented

cultures also exhibited pronounced cell aggregation (Fig. 5E), consistent with divalent-cation-induced flocculation in *Chlorella* systems (Vandamme et al., 2012). Such aggregation may generate localized microenvironments that influence lipid distribution, and Ca^{2+} exposure may also be associated with membrane-related remodeling and altered unsaturated fatty acid profiles (Shim et al., 2020). Within the TAP-based comparison, these results suggest that $CaCl_2$ treatment was associated with altered fatty acid accumulation and composition, particularly increased linoleic acid.

Combining the optimal cultivation medium (M2), Ca^{2+} adaptation, and D6 disruption (M2CaD6) yielded the highest total fatty acid content (32.23 ± 2.15 μg mg^{-1} DCW), representing a ~2.3-fold increase over TAPD6 (Fig. 5A). M2CaD6 also achieved the highest omega-3 accumulation (6.22 ± 0.42 μg mg^{-1} DCW) and omega-3 yield (14.90 ± 0.95 mg L^{-1}), corresponding to ~17-fold and ~20-fold increases over the original TAP-$CaCl_2$ protocol (PD0) (Preechaphonkul et al., 2024) in omega-3 content and yield, respectively (Fig. 5A-B). Total lipid content peaked at 22.63% DCW, consistent with the highest crude lipid yield (542.24 mg L^{-1}) among all tested conditions (Fig. 5D). When resolved into individual omega-3 components, the fatty acid profile was dominated by ALA, whereas EPA and DHA were detected at lower levels (Fig. 5C). When comparing $CaCl_2$-containing conditions, it should be noted that the $CaCl_2$-induced workflows evaluated in the present study (TAPCaD6 and M2CaD6) were designed with delayed $CaCl_2$ induction after the early growth phase, allowing biomass accumulation to proceed before induction treatment. This process configuration differed from the previously reported protocol (P), in which $CaCl_2$ was present throughout cultivation. Accordingly, these conditions are more appropriately interpreted as distinct process configurations than as directly equivalent physiological treatments. The marked improvement observed in M2CaD6 is therefore most reasonably understood as the outcome of the integrated workflow, although the specific contribution of each component cannot be quantitatively partitioned from the present design.

Table 1 provides a comparative benchmark of omega-3 performance in selected *Chlorella* studies. Despite methodological differences among studies, the M2CaD6 workflow showed competitive omega-3 content and yield, supporting the value of integrating cultivation optimization with cellulase-assisted extraction. In contrast to many previous studies that focused primarily on either cultivation performance or extraction improvement, the present workflow combined both stages within a single process framework. Cross-study comparison of extraction performance remains difficult because strain background, cultivation conditions, extraction protocols, and analytical methods differ substantially among studies. Previous CCD- and RSM-based studies likewise support the relevance of this integrated strategy, with cultivation-stage optimization improving biomass-related performance in *Chlorella* (Do et al., 2022; Rincon et al., 2024) and extraction-stage optimization enhancing lipid recovery in related systems (Hadrich et al., 2018). Recent *Chlorella*-based strain-improvement studies further suggest that process optimization alone may not fully define the upper limit of long-chain omega-3 production. In *Chlorella vulgaris*, chemical mutagenesis combined with adaptive laboratory evolution was reported to enhance EPA and DHA yields by 485% and 161%, respectively (Zhang et al., 2025). Likewise, UV mutagenesis followed by H_2O_2 treatment in *Chlorella* sp. was reported to enhance EPA and DHA content together with overall omega-3 fatty acid levels (Sivaramakrishnan and Incharoensakdi, 2023). Although these studies are not directly comparable with the present workflow in terms of strain background, intervention strategy, and reported response metrics, they indicate that future strain-improvement approaches may further extend the EPA/DHA potential of KLSc59 beyond what can be achieved by cultivation and extraction optimization.

To further probe stress-induced redirection of lipid metabolism, nitrogen was halved (M2CaND6) or combined with increased light intensity (M2CaNLD6). Nitrogen reduction did not improve total fatty acid content relative to M2CaD6 but shifted fatty acid composition toward SAT, MUFA, and LA with reduced omega-3 content, consistent with nitrogen-stress-driven lipid remodeling and altered desaturation dynamics (Hu et al., 2008; Wang and Miao, 2022; Vijayan et al., 2024). The marked increase in LA, a precursor for omega-3 biosynthesis, suggests potential downstream bottlenecks or timing effects in desaturation and elongation pathways.

Under combined nitrogen reduction and high light (M2CaNLD6), fatty acid content per DCW decreased substantially (Fig. 5A), yet rapid growth resulted in the highest fatty acid yield (128.18 ± 4.94 mg L^{-1}) and an omega-3 yield (14.22 ± 0.29 mg L^{-1}) comparable to that of M2CaD6 (Fig. 5B). Despite a relatively low lipid fraction (7.6% DCW), M2CaNLD6 still produced a substantial crude lipid yield of 407.21 mg L^{-1} (Fig. 5D). These results reflect a biomass-driven trade-off in which rapid growth partially compensated for reduced lipid accumulation per unit biomass under the combined nitrogen-reduction and high-light condition, consistent with previous reports that light intensity can influence the balance between proliferation and lipid storage in microalgae (Nzayisenga et al., 2020). This response may reflect multiple, non-exclusive mechanisms, including dilution of cellular lipid content by rapid biomass accumulation, altered carbon partitioning under high light, and possible oxidative stress. However, no direct measurements of reactive oxygen species (ROS) formation or lipid peroxidation were performed in the present study. Morphological differences observed under M2CaNLD6 (Fig. 5E) may reflect stress-associated physiological remodeling that coincided with reduced lipid accumulation per cell, consistent with nitrogen-stress-induced thylakoid and lipid remodeling reported in *Chlorella* (Vijayan et al., 2024; Wang and Miao, 2022). However, light effects remain context-dependent, as increased lipid accumulation has also been reported under nutrient-rich conditions (Palikrousis et al., 2024). Overall, M2CaD6 was the best-performing condition, achieving omega-3 accumulation per biomass while sustaining high omega-3 yield. Although M2CaNLD6 showed lower cellular lipid content, its omega-3 yield remained comparable, suggesting that biomass-driven strategies can compensate for reduced cellular lipid content under stress.

Direct cross-stage comparison between the biomass-stage optimization results and the subsequent comparative cultivation experiments should be interpreted cautiously, because the biomass-stage CCD was conducted under 50 µmol photons m^{-2} s^{-1}, whereas most comparative cultivation conditions in Section 3.4 were evaluated under 5 µmol photons m^{-2} s^{-1}. Within Section 3.4, the main comparative conditions (PD0, PD6, TAPD6, TAPCaD6, M2CaD6, and M2CaND6) were assessed under the same low-light framework, whereas M2CaNLD6 was intentionally evaluated under higher light intensity as a stress condition. Comparison between M2CaND6 and M2CaNLD6 is also limited because light intensity and nitrogen reduction were changed simultaneously rather than independently in a factorial design. Therefore, the observed differences between these two conditions are more appropriately interpreted as reflecting the combined effect of light intensity and nitrogen reduction. Although the present study does not establish whether the selected carbon and nitrogen sources, or the M2 formulation, would remain best-performing under an alternative light regime, the favorable growth responses observed during the screening and biomass-stage optimization experiments suggest that this nutrient combination may remain supportive of biomass production beyond the tested experimental framework.

In the present study, $CaCl_2$ induction and nitrogen reduction were examined as selected comparative conditions, whereas cellulase loading and sonication duration were optimized within the tested CCD range. $CaCl_2$ induction was examined at a single concentration (10 mM), and

nitrogen reduction was tested at one step-down level (50% of the original ammonium nitrate concentration), corresponding to selected experimental levels. Further studies using wider ranges of $CaCl_2$ concentration, nitrogen reduction, and extraction variables would strengthen process evaluation. An independent exhaustive solvent-extraction baseline was not established in the present study. Therefore, the extraction results should be interpreted primarily as comparative recovery within the tested extraction framework. Nevertheless, the observed differences among the tested conditions still support the comparative performance advantage of D6 under the present experimental conditions. The stress responses were assessed only at the end point, without direct mechanistic measurements to resolve nitrogen status, carbon partitioning, oxidative status, or photosynthetic dynamics. Time-resolved experiments in controlled photobioreactor systems will therefore be important for clarifying the mechanisms underlying omega-3 remodeling in *Chlorella* sp. KLSc59.

From a scale-up perspective, the acetate-based M2 strategy could potentially be adapted to fed-batch or semi-continuous operation, because controlled supplementation of organic carbon may support biomass accumulation while improving process stability in mixotrophic *Chlorella* systems (Xie et al., 2020; Dragone, 2022). Previous studies have shown that mixotrophic cultivation with organic carbon supplementation can improve *Chlorella* biomass productivity, and semi-continuous cultivation has been demonstrated as a practical strategy for maintaining stable production performance (Xie et al., 2020; Chen et al., 2019). The light conditions used in the present study were selected to support stage-specific process comparison and stress evaluation at laboratory scale, and should not be interpreted as direct operating targets for industrial photobioreactors. Further validation under reactor-relevant light delivery conditions will therefore be required to evaluate the transferability of the present workflow to large-scale cultivation. At the same time, the direct large-scale application of standard TAP-based media may be constrained by medium cost, and further optimization of medium composition will likely be required to improve economic feasibility. In this context, the present study provides useful direction by demonstrating that acetic acid, ammonium nitrate, and pH, together with $CaCl_2$ adaptation, significantly influenced both biomass accumulation and intracellular fatty acid profiles in *Chlorella* sp. KLSc59. These findings suggest that future medium development should not only aim to reduce formulation cost, but also retain those key factors that govern biomass productivity and omega-3-associated lipid accumulation. Although the present workflow substantially improved omega-3 content and yield relative to the previous KLSc59 protocol, the resulting production levels should still be interpreted as laboratory-scale outcomes, and further increases in volumetric productivity would be required before industrial feasibility can be assessed.

Likewise, the performance of the cellulase-assisted sonication strategy has important implications for process development at larger scale. Enzymatic pretreatment likely reduced the structural resistance of the carbohydrate-rich cell wall, thereby decreasing the mechanical severity required for subsequent disruption, which may help reduce the potential risk of oxidative degradation of polyunsaturated fatty acids during extraction (Lee et al., 2017; Liu et al., 2022). In this context, the combination of cellulase with moderate sonication may offer a more practical balance than reliance on prolonged or high-intensity sonication alone, because excessive mechanical input can increase energy demand and may promote local heating and oxidative degradation of sensitive fatty acids (Lee et al., 2017; Liu et al., 2022). Nevertheless, cellulase loading remains an important economic consideration for process translation, and further optimization will be required to balance enzyme dosage, extraction efficiency, and operating cost under scaled-up conditions (Lee et al., 2017; Dragone, 2022). The cellulase loading used here

should be interpreted as a laboratory-scale process condition selected to maximize recovery within the tested design space, rather than as an economically validated dosage for large-scale operation. Because enzymatic hydrolysis efficiency depends jointly on enzyme dosage and incubation time, future scale-up studies may benefit from re-optimizing this trade-off by evaluating whether lower cellulase loading can be compensated by longer hydrolysis time under reactor-relevant conditions. Beyond process development, the present extraction workflow may also serve as a useful laboratory framework for improving comparative fatty-acid profiling and omega-3 characterization in *Chlorella* biomass.

4. CONCLUSION

This study established a strain-specific integrated bioprocess for enhancing omega-3 oil production and recovery from *Chlorella* sp. KLSc59. Acetic acid and ammonium nitrate were identified as the best-performing carbon and nitrogen sources under the tested screening conditions. The CCD-guided biomass-stage optimization identified M2 (33.9 mM acetic acid, 16.1 mM ammonium nitrate, pH 6.6) as the best-performing cultivation condition within the investigated design space. A second CCD-based analysis identified D6 (1,000 IU g^{-1} DCW cellulase; 150 s sonication) as the best-performing disruption condition within the tested range, with improved fatty acid recovery under the tested extraction conditions. The combination of M2 cultivation, $CaCl_2$ induction, and D6 extraction (M2CaD6) gave the highest cellular omega-3 content (6.22 µg mg^{-1} DCW) and yield (14.90 mg L^{-1}), representing ~17-fold and ~20-fold increases over the PD0 protocol, respectively. Stress experiments showed that nitrogen reduction mainly altered fatty acid composition, whereas nitrogen reduction combined with higher light intensity enhanced total fatty acid yield despite lower lipid content per unit biomass. Overall omega-3 enhancement was driven predominantly by ALA, suggesting limited conversion to EPA and DHA. Further time-course profiling and strain-improvement approaches are therefore recommended.

Supplementary data associated with this article are available in the online version and include additional methodological and statistical details supporting the CCD analyses.

REFERENCES

Adams, C., Godfrey, V., Wahlen, B., Seefeldt, L., Bugbee, B. 2013. Understanding precision nitrogen stress to optimize the growth and lipid content tradeoff in oleaginous green microalgae. *Bioresource Technology*, 131, 188–194.

Adarme-Vega, T.C., Lim, D.K., Timmins, M., Vernen, F., Li, Y., Schenk, P.M. 2012. Microalgal biofactories: a promising approach towards sustainable omega-3 fatty acid production. *Microbial cell factories*, 11(1), 96.

Alavijeh, R.S., Karimi, K., Wijffels, R.H., van Den Berg, C., Eppink, M. 2020. Combined bead milling and enzymatic hydrolysis for efficient fractionation of lipids, proteins, and carbohydrates of *Chlorella vulgaris* microalgae. *Bioresource Technology*, 309, 123321.

Andersen, R.A. 2005. *Algal culturing techniques*. Elsevier.

Batista, A.P., Gouveia, L., Bandarra, N.M., Franco, J.M., Raymundo, A. 2013. Comparison of microalgal biomass profiles as novel functional ingredient for food products. *Algal Research*, 2(2), 164–173.

Bligh, E.G., Dyer, W.J. 1959. A rapid method of total lipid extraction and purification. *Canadian journal of biochemistry and physiology*, 37(8), 911–917.

Cai, Y., Zhai, L., Wu, K., Li, Z., Gu, Z., Wang, Y., Cui, X., Zhou, T., Ruan, R., Liu, T. 2022. Mechanisms of promotion in the heterotrophic growth of *Chlorella vulgaris* by the combination of sodium acetate and hydrolysate of broken rice. *Bioresource technology*, 364, 127965.

Canelli, G., Tarnutzer, C., Carpine, R., Neutsch, L., Bolten, C.J., Dionisi, F., Mathys, A. 2020. Biochemical and nutritional evaluation of *Chlorella* and *Auxenochlorella* biomasses relevant for food application. *Frontiers in Nutrition*, 7, 565996.

Catalanotti, C., Yang, W., Posewitz, M.C., Grossman, A.R. 2013. Fermentation metabolism and its evolution in algae. *Frontiers in plant science*, 4, 150.

Cecchin, M., Benfatto, S., Griggio, F., Mori, A., Cazzaniga, S., Vitulo, N., Delledonne, M., Ballottari, M. 2018. Molecular basis of autotrophic vs mixotrophic growth in *Chlorella sorokiniana*. *Scientific Reports*, 8(1), 6465.

Chen, J.-H., Chen, C.-Y., Hasunuma, T., Kondo, A., Chang, C.-H., Ng, I.-S., Chang, J.-S. 2019. Enhancing lutein production with mixotrophic cultivation of *Chlorella sorokiniana* MB-1-M12 using different bioprocess operation strategies. *Bioresource technology*, 278, 17–25.

Chen, Y.-H., Walker, T.H. 2011. Biomass and lipid production of heterotrophic microalgae *Chlorella* protothecoides by using biodiesel-derived crude glycerol. *Biotechnology letters*, 33(10), 1973–1983.

Chen, Z., Wang, L., Qiu, S., Ge, S. 2018. Determination of microalgal lipid content and fatty acid for biofuel production. *BioMed research international*, 2018(1), 1503126.

Cho, H.-S., Oh, Y.-K., Park, S.-C., Lee, J.-W., Park, J.-Y. 2013. Effects of enzymatic hydrolysis on lipid extraction from *Chlorella vulgaris*. *Renewable Energy*, 54, 156–160.

Darwish, R., Gedi, M.A., Akepach, P., Assaye, H., Zaky, A.S., Gray, D.A. 2020. *Chlamydomonas reinhardtii* is a potential food supplement with the capacity to outperform *Chlorella* and *Spirulina*. *Applied Sciences*, 10(19), 6736.

Dickson, A.G., Sabine, C.L., Christian, J.R. 2007. Guide to best practices for ocean CO2 measurements.

Do, C.V.T., Nguyen, N.T.T., Pham, M.H.T., Pham, T.Y.T., Ngo, V.G., Le, T.G., Tran, T.D. 2022. Central composite design for simultaneously optimizing biomass and lutein production by

a mixotrophic *Chlorella sorokiniana* TH01. *Biochemical Engineering Journal*, 177, 108231.

Dragone, G. 2022. Challenges and opportunities to increase economic feasibility and sustainability of mixotrophic cultivation of green microalgae of the genus *Chlorella*. *Renewable and Sustainable Energy Reviews*, 160, 112284.

Harris, E.H. 1989. The *Chlamydomonas* sourcebook: a comprehensive guide to biology and laboratory use, Academic Press, San Diego.

Ellison, C.R., Overa, S., Boldor, D. 2019. Central composite design parameterization of microalgae/cyanobacteria co-culture pretreatment for enhanced lipid extraction using an external clamp-on ultrasonic transducer. *Ultrasonics Sonochemistry*, 51, 496–503.

FAO. 2024. *The State of World Fisheries and Aquaculture 2024*. Blue Transformation in action, Rome.

Geada, P., Francisco, D., Pereira, F., Maciel, F., Madureira, L., Barros, A., Silva, J.L., Vicente, A.A., Teixeira, J.A. 2023. Multivariable optimization process of heterotrophic growth of *Chlorella vulgaris*. *Food and Bioproducts Processing*, 138, 1–13.

Gerde, J.A., Montalbo-Lomboy, M., Yao, L., Grewell, D., Wang, T. 2012. Evaluation of microalgae cell disruption by ultrasonic treatment. *Bioresource technology*, 125, 175–181.

Giordano, M., Beardall, J., Raven, J.A. 2005. CO_2 concentrating mechanisms in algae: mechanisms, environmental modulation, and evolution. *Annu. Rev. Plant Biol.*, 56(1), 99–131.

Goncalves, E.C., Johnson, J.V., Rathinasabapathi, B. 2013. Conversion of membrane lipid acyl groups to triacylglycerol and formation of lipid bodies upon nitrogen starvation in biofuel green algae *Chlorella* UTEX29. *Planta*, 238(5), 895–906.

González-Garcinuño, Á., Tabernero, A., Sánchez-Álvarez, J.M., Del Valle, E.M.M., Galán, M.A. 2014. Effect of nitrogen source on growth and lipid accumulation in *Scenedesmus abundans* and *Chlorella ellipsoidea*. *Bioresource technology*, 173, 334–341.

Gorman, D.S., Levine, R. 1965. Cytochrome f and plastocyanin: their sequence in the photosynthetic electron transport chain of *Chlamydomonas reinhardi*. *Proceedings of the National Academy of Sciences*, 54(6), 1665–1669.

Guckert, J.B., Cooksey, K.E. 1990. Triglyceride accumulation and fatty acid profile changes in *Chlorella* (Chlorophyta) during high Ph-induced cell cycle Inhibition 1. *Journal of Phycology*, 26(1), 72–79.

Günerken, E., D'Hondt, E., Eppink, M., Garcia-Gonzalez, L., Elst, K., Wijffels, R.H. 2015. Cell disruption for microalgae biorefineries. *Biotechnology advances*, 33(2), 243–260.

Guo, X., Su, G., Li, Z., Chang, J., Zeng, X., Sun, Y., Lu, Y., Lin, L. 2015. Light intensity and N/P nutrient affect the accumulation of lipid and unsaturated fatty acids by *Chlorella* sp. *Bioresource technology*, 191, 385–390.

Hadrich, B., Akremi, I., Dammak, M., Barkallah, M., Fendri, I., Abdelkafi, S. 2018. Optimization of lipids' ultrasonic extraction and production from *Chlorella* sp. using response-surface methodology. *Lipids in Health and Disease*, 17(1), 87.

Hattori, A. 1957. Studies on the metabolism of urea and other nitrogenous compounds in *Chlorella ellipsoidea* I. Assimilation of urea and other nitrogenous compounds by nitrogen-starved cells. *The journal of Biochemistry*, 44(5), 253–273.

Heredia-Arroyo, T., Wei, W., Ruan, R., Hu, B. 2011. Mixotrophic cultivation of *Chlorella vulgaris* and its potential application for the oil accumulation from non-sugar materials. *Biomass and bioenergy*, 35(5), 2245–2253.

Hixson, S.M., Sharma, B., Kainz, M.J., Wacker, A., Arts, M.T. 2015. Production, distribution, and abundance of long-chain omega-3 polyunsaturated fatty acids: a fundamental dichotomy between freshwater and terrestrial ecosystems. *Environmental Reviews*, 23(4), 414–424.

Hu, Q., Sommerfeld, M., Jarvis, E., Ghirardi, M., Posewitz, M., Seibert, M., Darzins, A. 2008. Microalgal triacylglycerols as feedstocks for biofuel production: perspectives and advances. *The plant journal*, 54(4), 621–639.

Innes, J.K., Calder, P.C. 2020. Marine omega-3 (N-3) fatty acids for cardiovascular health: an update for 2020. *International journal of molecular sciences*, 21(4), 1362.

John, P., Syrett, P. 1967. The purification and properties of isocitrate lyase from *Chlorella*. *Biochemical Journal*, 105(1), 409–416.

Lacroux, J., Seira, J., Trably, E., Bernet, N., Steyer, J.-P., van Lis, R. 2021. Mixotrophic growth of *Chlorella sorokiniana* on acetate and butyrate: interplay between substrate, C: N ratio and pH. *Frontiers in microbiology*, 12, 703614.

Lacroux, J., Trably, E., Bernet, N., Steyer, J.-P., van Lis, R. 2020. Mixotrophic growth of microalgae on volatile fatty acids is determined by their undissociated form. *Algal Research*, 47, 101870.

Lee, S.Y., Cho, J.M., Chang, Y.K., Oh, Y.-K. 2017. Cell disruption and lipid extraction for microalgal biorefineries: A review. *Bioresource technology*, 244, 1317–1328.

Liang, K., Zhang, Q., Cong, W. 2012. Enzyme-assisted aqueous extraction of lipid from microalgae. *Journal of Agricultural and Food Chemistry*, 60(47), 11771–11776.

Liang, Y., Sarkany, N., Cui, Y. 2009. Biomass and lipid productivities of *Chlorella vulgaris* under autotrophic, heterotrophic and mixotrophic growth conditions. *Biotechnology letters*, 31(7), 1043–1049.

Liu, T., Chen, Z., Xiao, Y., Yuan, M., Zhou, C., Liu, G., Fang, J., Yang, B. 2022a. Biochemical and morphological changes triggered by nitrogen stress in the oleaginous microalga *Chlorella vulgaris*. *Microorganisms*, 10(3), 566.

Liu, T., Li, Y., Liu, F., Wang, C. 2016. The enhanced lipid accumulation in oleaginous microalga by the potential continuous nitrogen-limitation (CNL) strategy. *Bioresource technology*, 203, 150–159.

Liu, Y., Liu, X., Cui, Y., Yuan, W. 2022b. Ultrasound for microalgal cell disruption and product extraction: A review. *Ultrasonics Sonochemistry*, 87, 106054.

Maltsev, Y., Kulikovskiy, M., Maltseva, S. 2023. Nitrogen and phosphorus stress as a tool to induce lipid production in microalgae. *Microbial cell factories*, 22(1), 239.

Manhaeghe, D., Blomme, T., Van Hulle, S., Rousseau, D. 2020. Experimental assessment and mathematical modelling of the growth of *Chlorella vulgaris* under photoautotrophic, heterotrophic and mixotrophic conditions. *Water Research*, 184, 116152.

Markou, G., Dao, L.H., Muylaert, K., Beardall, J. 2017. Influence of different degrees of N limitation on photosystem II performance and heterogeneity of *Chlorella vulgaris*. *Algal research*, 26, 84–92.

Miazek, K., Kratky, L., Sulc, R., Jirout, T., Aguedo, M., Richel, A., Goffin, D. 2017. Effect of organic solvents on microalgae growth, metabolism and industrial bioproduct extraction: a review. *International journal of molecular sciences*, 18(7), 1429.

Miller, P.E., Van Elswyk, M., Alexander, D.D. 2014. Long-chain omega-3 fatty acids eicosapentaenoic acid and docosahexaenoic acid and blood pressure: a meta-analysis of randomized controlled trials. *American journal of hypertension*, 27(7), 885–896.

Moradi-Kheibari, N., Ahmadzadeh, H., Lyon, S.R. 2022. Correlation of total lipid content of *Chlorella vulgaris* with the dynamics of individual fatty acid growth rates. *Frontiers in Marine Science*, 9, 837067.

Morris, I., Syrett, P. 1963. The development of nitrate reductase in *Chlorella* and its repression by ammonium. *Archiv für Mikrobiologie*, 47(1), 32–41.

Mujtaba, G., Choi, W., Lee, C.-G., Lee, K. 2012. Lipid production by *Chlorella vulgaris* after a shift from nutrient-rich to nitrogen starvation conditions. *Bioresource technology*, 123, 279–283.

Natto, Z.S., Yaghmoor, W., Alshaeri, H.K., Van Dyke, T.E. 2019. Omega-3 fatty acids effects on inflammatory biomarkers and lipid profiles among diabetic and cardiovascular disease patients: a systematic review and meta-analysis. *Scientific reports*, 9(1), 18867.

Nayak, M., Suh, W.I., Chang, Y.K., Lee, B. 2019. Exploration of two-stage cultivation strategies using nitrogen starvation to maximize the lipid productivity in *Chlorella* sp. HS2. *Bioresource technology*, 276, 110–118.

Nzayisenga, J.C., Farge, X., Groll, S.L., Sellstedt, A. 2020. Effects of light intensity on growth and lipid production in microalgae grown in wastewater. *Biotechnology for biofuels*, 13(1), 4.

Oh, Y.-K., Kim, S., Ilhamsyah, D.P.A., Lee, S.-G., Kim, J.R. 2022. Cell disruption and lipid extraction from *Chlorella* species for biorefinery applications: Recent advances. *Bioresource Technology*, 366, 128183.

Palikrousis, T.L., Manolis, C., Kalamaras, S.D., Samaras, P. 2024. Effect of light intensity on the growth and nutrient uptake of the microalga *Chlorella sorokiniana* cultivated in biogas plant digestate. *Water*, 16(19), 2782.

Perez-Garcia, O., Escalante, F.M., De-Bashan, L.E., Bashan, Y. 2011a. Heterotrophic cultures of microalgae: metabolism and potential products. *Water research*, 45(1), 11–36.

Perez-Garcia, O., Bashan, Y., Esther Puente, M. 2011b. Organic carbon supplementation of sterilized municipal wastewater is essential for heterotrophic growth and removing ammonium by the microalga *Chlorella vulgaris* 1. *Journal of phycology*, 47(1), 190–199.

Pozzobon, V., Cui, N., Moreaud, A., Michiels, E., Levasseur, W. 2021. Nitrate and nitrite as mixed source of nitrogen for *Chlorella vulgaris*: Growth, nitrogen uptake and pigment contents. *Bioresource technology*, 330, 124995.

Preechaphonkul, N., Sirikwanpong, S., Maneeruttanarungroj, C. 2024. Freshwater green alga *Chlorella* sp. KLSc59 produced all forms of omega-3 oil: ALA, EPA, and DHA. *Algal Research*, 80, 103532.

Qiu, R., Gao, S., Lopez, P.A., Ogden, K.L. 2017. Effects of pH on cell growth, lipid production and CO_2 addition of microalgae *Chlorella sorokiniana*. *Algal research*, 28, 192–199.

Rahman, M.M., Hosano, N., Hosano, H. 2022. Recovering microalgal bioresources: a review of cell disruption methods and extraction technologies. *Molecules*, 27(9), 2786.

Rees, T., Syrett, P. 1984. Proton cotransport of thiourea in *Chlorella fusca*. *FEMS microbiology letters*, 25(1), 17–19.

Rincon, S.M., Beyenal, H., Romero, H.M. 2024. A response surface methodology study for *Chlorella vulgaris* mixotrophic culture optimization. *Microorganisms*, 12(2), 379.

Ritchie, R.J. 2008. Universal chlorophyll equations for estimating chlorophylls a, b, c, and d and total chlorophylls in natural assemblages of photosynthetic organisms using acetone, methanol, or ethanol solvents. *Photosynthetica*, 46(1), 115–126.

Scherholz, M.L., Curtis, W.R. 2013. Achieving pH control in microalgal cultures through fed-batch addition of stoichiometrically-balanced growth media. *BMC biotechnology*, 13(1), 39.

Sekine, M., Yoshida, A., Akizuki, S., Kishi, M., Toda, T. 2020. Microalgae cultivation using undiluted anaerobic digestate by introducing aerobic nitrification–desulfurization treatment. *Water Science and Technology*, 82(6), 1070–1080.

Shelp, B.J., Canvin, D.T. 1980. Utilization of exogenous inorganic carbon species in photosynthesis by *Chlorella pyrenoidosa*. *Plant Physiology*, 65(5), 774–779.

Shi, T.-Q., Wang, L.-R., Zhang, Z.-X., Sun, X.-M., Huang, H. 2020. Stresses as first-line tools for enhancing lipid and carotenoid production in microalgae. *Frontiers in bioengineering and biotechnology*, 8, 610.

Shim, S.J., Hong, M.E., Chang, W.S., Sim, S.J. 2020. Repeated-batch production of omega-3 enriched biomass of *Chlorella sorokiniana* via calcium-induced homeoviscous adaptation. *Bioresource technology*, 303, 122944.

Sirawattanamongkol, T., Maswanna, T., Maneeruttanarungroj, C. 2020. A newly isolated green alga *Chlorella* sp. KLSc59: potential for biohydrogen production. *Journal of Applied Phycology*, 32(5), 2927–2936.

Sivaramakrishnan, R., Incharoensakdi, A. 2023. UV mutagenesis followed by hydrogen peroxide treatment ameliorates lipid production and omega-3 fatty acids levels in *Chlorella* sp. *Algal Research*, 74, 103195.

Sueoka, N. 1960. Mitotic replication of deoxyribonucleic acid in *Chlamydomonas reinhardi*. *Proceedings of the National Academy of Sciences*, 46(1), 83–91.

Syrett, P., Morris, I. 1963. The inhibition of nitrate assimilation by ammonium in *Chlorella*. *Biochimica et Biophysica Acta (BBA)-Specialized Section on Enzymological Subjects*, 67, 566–575.

Vandamme, D., Foubert, I., Fraeye, I., Meesschaert, B., Muylaert, K. 2012. Flocculation of *Chlorella vulgaris* induced by high pH: role of magnesium and calcium and practical implications. *Bioresource technology*, 105, 114–119.

Vijayan, J., Wase, N., Liu, K., Morse, W., Zhang, C., Riekhof, W.R. 2024. ROS-mediated thylakoid membrane remodeling and triacylglycerol biosynthesis under nitrogen starvation in the alga *Chlorella sorokiniana*. *Frontiers in Plant Science*, 15, 1418049.

Visciano, P. 2024. Environmental contaminants in fish products: Food safety issues and remediation strategies. *Foods*, 13(21), 3511.

Wang, J., Zhou, W., Chen, H., Zhan, J., He, C., Wang, Q. 2019a. Ammonium nitrogen tolerant *Chlorella* strain screening and its damaging effects on photosynthesis. *Frontiers in microbiology*, 9, 3250.

Wang, R., Miao, X. 2022. Lipid turnover and SQUAMOSA promoter-binding proteins mediate variation in fatty acid desaturation under early nitrogen deprivation revealed by lipidomic and transcriptomic analyses in *Chlorella pyrenoidosa*. *Frontiers in Plant Science*, 13, 987354.

Wang, T., Zhang, X., Zhou, N., Shen, Y., Li, B., Chen, B.E., Li, X. 2023. Association Between Omega-3 Fatty Acid Intake and Dyslipidemia: A Continuous Dose–Response Meta-Analysis of Randomized Controlled Trials. *Journal of the American Heart Association*, 12(11), e029512.

Wang, X., Fosse, H.K., Li, K., Chauton, M.S., Vadstein, O., Reitan, K.I. 2019b. Influence of nitrogen limitation on lipid accumulation and EPA and DHA content in four marine microalgae for possible use in aquafeed. *Frontiers in Marine Science*, 6, 95.

Weber, S., Grande, P.M., Blank, L.M., Klose, H. 2022. Insights into cell wall disintegration of *Chlorella vulgaris*. *PLoS One*, 17(1), e0262500.

Xie, Z., Lin, W., Liu, J., Luo, J. 2020. Mixotrophic cultivation of *Chlorella* for biomass production by using pH-stat culture medium: Glucose-Acetate-Phosphorus (GAP). *Bioresource technology*, 313, 123506.

Zeebe, R.E., Wolf-Gladrow, D. 2001. *CO2 in seawater: equilibrium, kinetics, isotopes*. Gulf Professional Publishing.

Zibarev, N., Toumi, A., Politaeva, N., Iljin, I. 2024. Nutrients recovery from dairy wastewater by *Chlorella vulgaris* and comparison of the lipid's composition with various *Chlorella* strains for biodiesel production. *Plos one*, 19(4), e0297464.

Zhang, J., Wu, G., Lu, F., Wu, G., Wang, X., Li, Y., Xu, R., Zhou, J., Cai, X., Liu, Z. 2025. Enhancing EPA and DHA synthesis in acetic acid-supplemented *Chlorella vulgaris*: A combined strategy of chemical mutagenesis and adaptive laboratory evolution. *Chemical Engineering Journal*, 515, 163473.

Ziganshina, E.E., Bulynina, S.S., Ziganshin, A.M. 2022. Growth characteristics of *Chlorella sorokiniana* in a photobioreactor during the utilization of different forms of nitrogen at various temperatures. *Plants*, 11(8), 1086.

Zuorro, A., Malavasi, V., Cao, G., Lavecchia, R. 2019. Use of cell wall degrading enzymes to improve the recovery of lipids from *Chlorella sorokiniana*. *Chemical Engineering Journal*, 377, 120325.

Zych, M., Burczyk, J., Borymska, W., Kaczmarczyk-Sedlak, I. 2022. Accumulation of proteins in the medium of the various naturally occurring *Chlorella* and *Scenedesmus* microalgae containing and not-containing algaenan. *Algal Research*, 62, 102598.

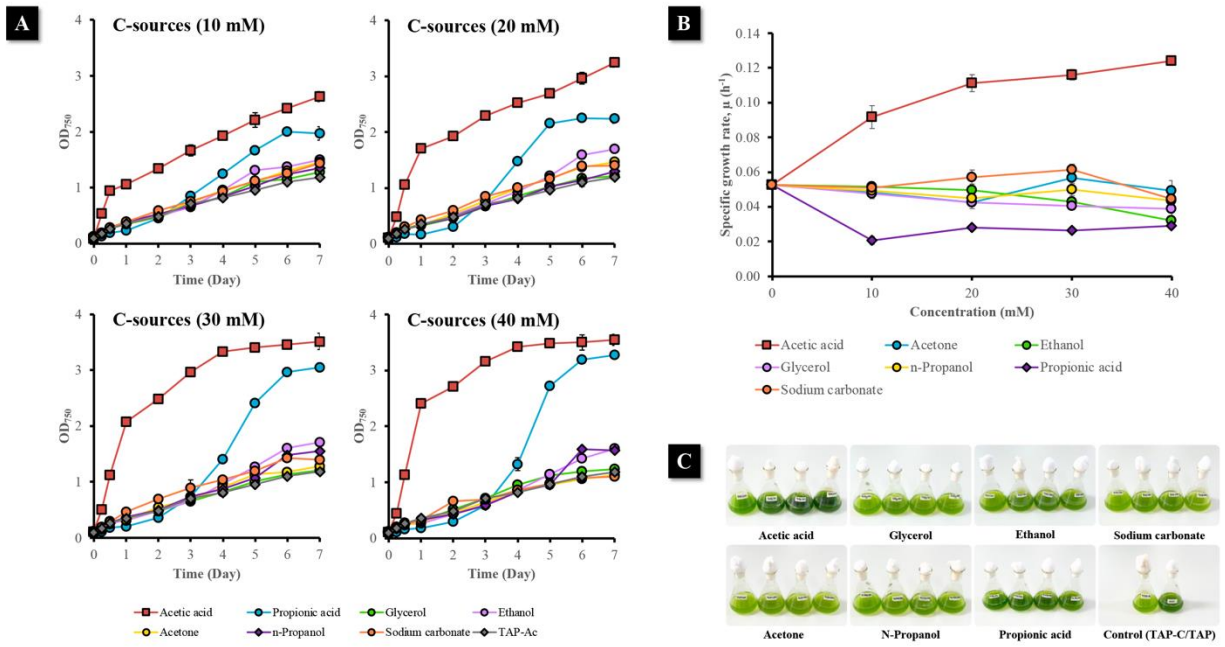

Fig. 1 Carbon source optimization for microalgal cultivation: (A) Growth curves at different carbon concentrations (10, 20, 30, and 40 mM), (B) Specific growth rate at various carbon concentrations, and (C) Visual appearance of cultures on day 7. Error bars represent means ± standard deviations from biological triplicates.

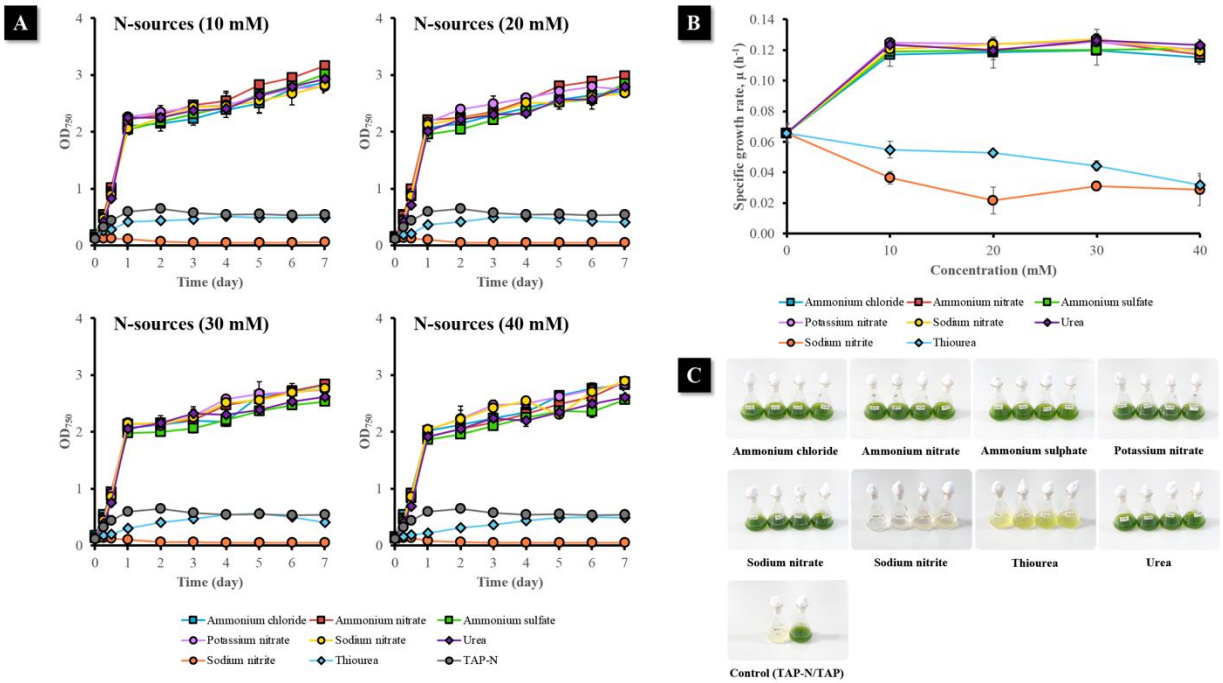

Fig. 2 Nitrogen source optimization for microalgal cultivation: (A) Growth curves at different nitrogen concentrations (10, 20, 30, and 40 mM), (B) Specific growth rate at various nitrogen concentrations, and (C) Visual appearance of cultures on day 7. Error bars represent means ± standard deviations from biological triplicates.

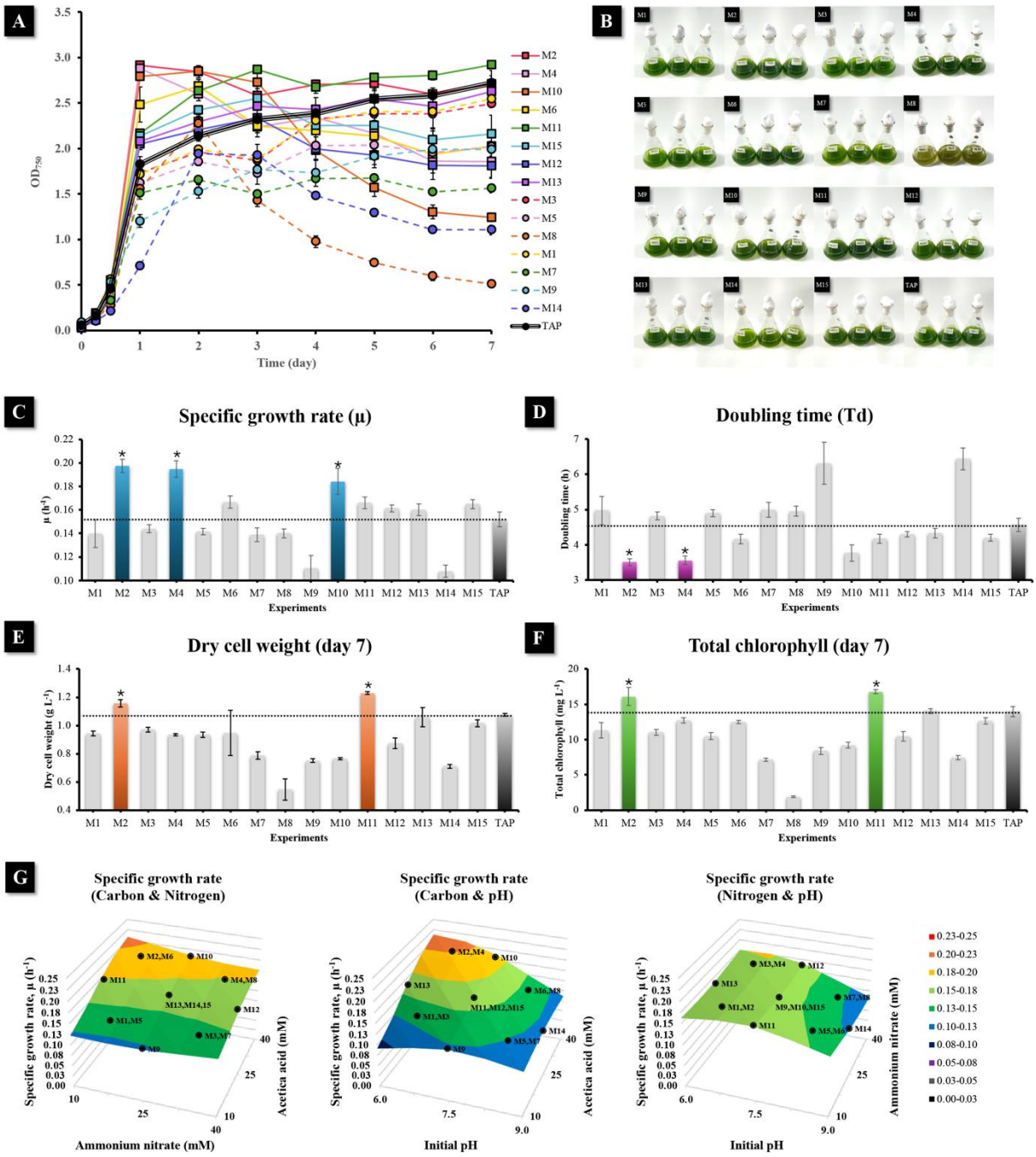

Fig. 3 Optimization of biomass growth using CCD. (A) Growth curves of *Chlorella* sp. KLSc59 under CCD conditions (M1-M15) over 7 days, monitored by OD_{750}. (B) Visual appearance of cultures on day 7. (C) Specific growth rate. (D) Doubling time. (E) Dry cell weight on day 7. (F) Total chlorophyll content on day 7. (G) Response surface plots showing the interaction effects of acetic acid concentration, ammonium nitrate concentration, and pH on specific growth rate, with observed experimental data points overlaid on the fitted surfaces. Error bars represent means ± standard deviations from biological triplicates. Asterisks (*) indicate the condition(s) belonging to the best-performing Tukey group within each panel ($p < 0.05$).

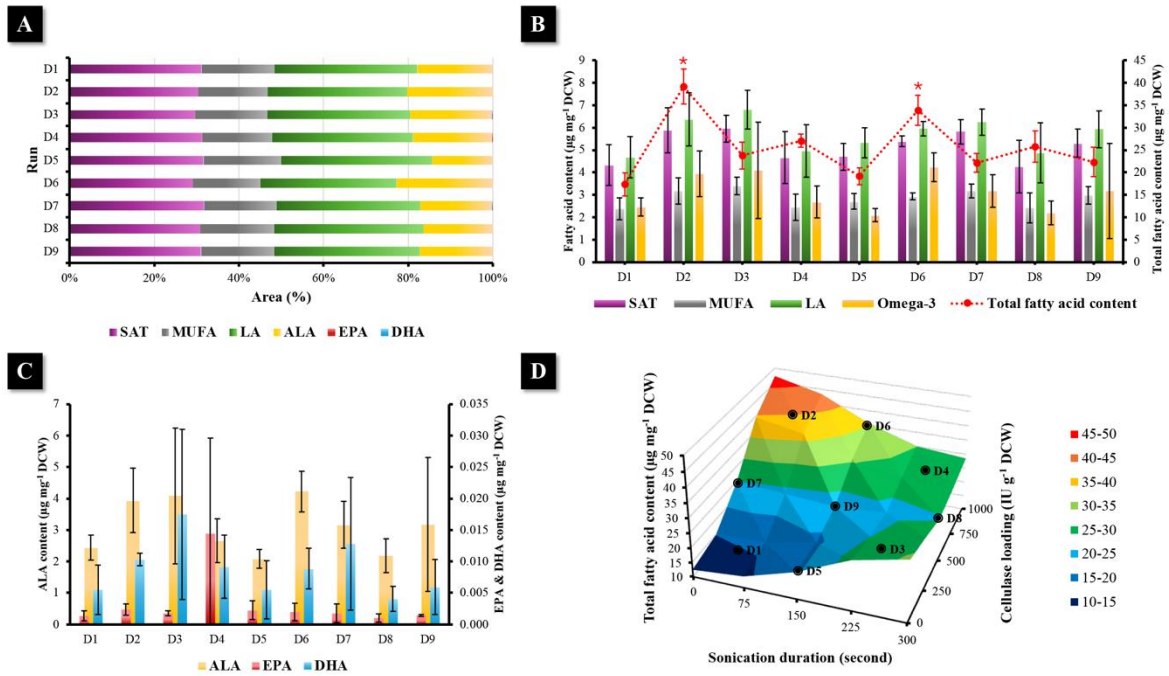

Fig. 4 Optimization of cell disruption and lipid extraction using CCD. (A) Fatty acid profiles of *Chlorella* sp. KLSc59 under different conditions (D1-D9), expressed as area percentage (%), including SAT, MUFA, LA, and the individual omega-3 fatty acids ALA, EPA, and DHA. (B) Total fatty acid content and selected fatty acid contents (SAT, MUFA, LA, and total omega-3) under each disruption condition. (C) Contents of the individual omega-3 fatty acids ALA, EPA, and DHA under each disruption condition; ALA is shown on the left y-axis, whereas EPA and DHA are shown on the right y-axis. (D) Response surface plots showing the interaction effects of cellulase loading and sonication duration on total fatty acid content, with observed experimental data points overlaid on the fitted surfaces. Error bars represent means ± standard deviations from biological triplicates. Asterisks (*) indicate the condition(s) belonging to the best-performing Tukey group within each panel ($p < 0.05$).

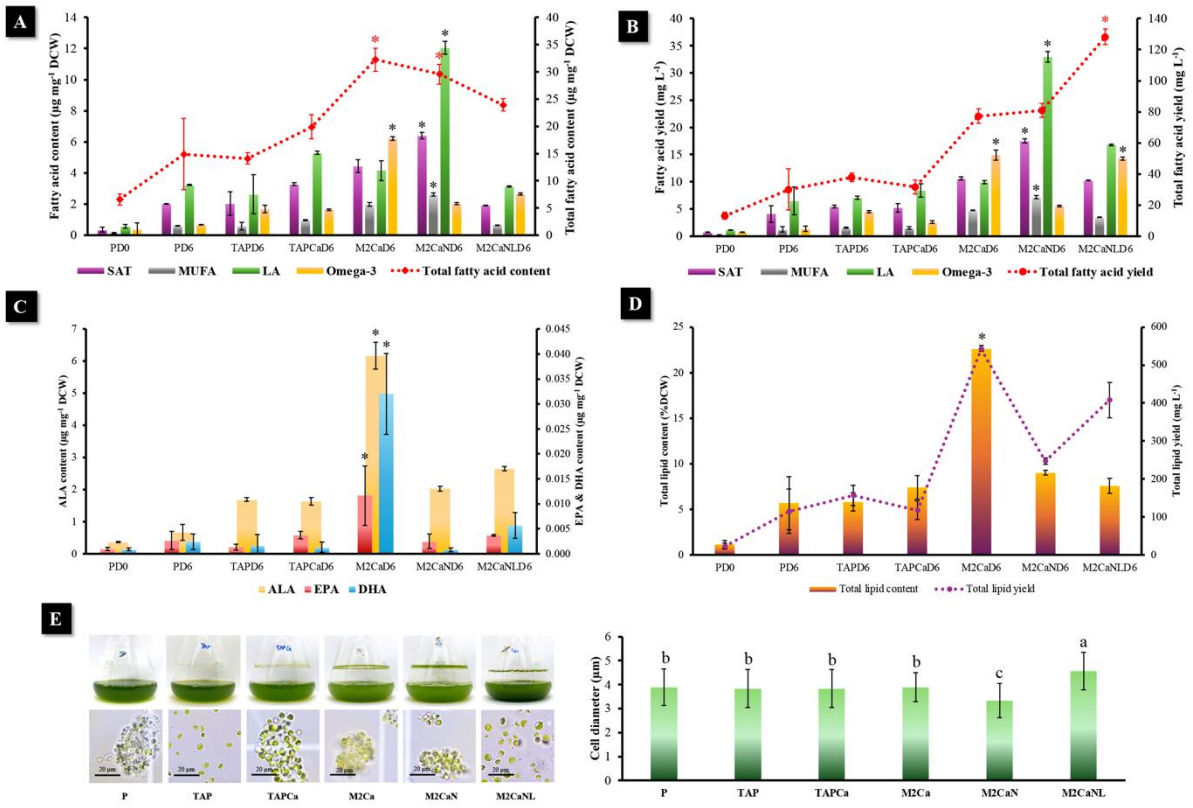

Fig. 5 Comparison of fatty acid, omega-3, and crude lipid production of *Chlorella* sp. KLSc59 under different cultivation and disruption strategies. (A) Selected fatty acid class contents (SAT, MUFA, LA, and total omega-3) and total fatty acid content. (B) Selected fatty acid class yields (SAT, MUFA, LA, and total omega-3) and total fatty acid yield. (C) Individual omega-3 fatty acid contents (ALA, EPA, and DHA). (D) Total lipid content and total lipid yield. (E) Bright-field micrographs and mean cell diameter on the final cultivation day. Error bars represent means ± standard deviations of biological triplicates. Different letters indicate Tukey groupings among all conditions within each panel ($p < 0.05$), whereas asterisks (*) mark the condition(s) belonging to the best-performing Tukey group in that panel.

Table 1 Comparative benchmark of omega-3 content and yield reported for selected *Chlorella* studies under different cultivation and extraction strategies.

***Chlorella* Species**	**Culture Medium / Conditions**	**Cell Disruption & Lipid Extraction**	**omega-3 content (%TFA)**	**omega-3 Content (µg mg^{-1} DCW)**	**omega-3 yield (mg L^{-1})**	**Total Fatty Acid Content (µg mg^{-1} DCW)**	**Cultivation Time**	**Reference**
Chlorella sp. KLSc59	Modified TAP (M2) + 10 mM $CaCl_2$ adaptation (M2CaD6)	Cellulase + sonication (D6: 1,000 IU g^{-1} DCW cellulase; 150 s sonication) + GC analysis	19.30%	6.22 ± 0.42	14.90 ± 0.95	32.23 ± 2.15	6 days	This study
Chlorella vulgaris INETI 58	Sorokin and Krauss medium; 25 °C; low light (150 µE m^{-2} s^{-1}); bubbling filtered air	Total lipids by Soxhlet with petroleum ether after 4 N HCl acid digestion; FAMEs by Acid catalysis (acetylchloride:methanol) at 80 °C for 1 h	19.95%	6.96	NR	34.89	NR (Harvested at stationary growth phase)	Batista et al. (2013)
Chlorella sp. (Commercial)	Grown autotrophically in open freshwater ponds (South China)	Folch method; cells were milled with mini bead beater	23.34% (only ALA)	11.6 ± 0.2 (ALA)	NR	49.7 (Calculated from SFA + USFA)	NR	Darwish et al. (2020)
Chlorella vulgaris (Strain CCALA 256)	Heterotrophic: Modified BBM + 15 g/L Glucose; 28 °C; dissolved oxygen tension was kept above 75%; aeration (4 L min−1); pH 7; 300 rpm	Freeze-dried; direct trans-esterification	19.7% (only ALA)	15.76 (ALA)	NR	80	7 days	Canelli et al. (2020)

Note: NR, not reported; ALA, indicates that only ALA was reported as the omega-3 component. Some absolute values were calculated from reported composition and/or total fatty acid content.